Selective Motion Control of a Crawling Magnetic Robot System for Wireless Self-Expandable Stent Delivery in Narrowed Tubular Environments

Wonseo Lee, *Student Member, IEEE*, Jaekwang Nam, Bongjun Jang, and Gunhee Jang, *Member, IEEE*

***Abstract*—A novel crawling magnetic robot system manipulated by a magnetic navigation system is proposed for wireless self-expandable stent delivery in narrowed tubular environments. The crawling magnetic robot is composed of a crawling module to generate crawling motion for navigation in a tubular environment, and a magnetic pulley module to generate drilling motion to unclog the blocked region and uncovering motion of a stent cover for the self-expandable stent deployment. The magnetic navigation system composed of three orthogonal pairs of electromagnetic coils can generate three dimensional external magnetic field by controlling the applied current. We also proposed selective motion control methods and design processes with fabrication. Finally, we prototyped the proposed crawling magnetic robot and conducted several experiments to show the validity of the proposed crawling magnetic robot and its manipulation methods.**

***Index Terms*—Crawling robot, magnetic navigation system, magnetic pulley, magnetic robot, self-expandable stent, stent delivery.**

LIST OF ACRONYMS

CMR	Crawling magnetic robot
EMF	External magnetic field
HC	Helmholtz coil
MNS	Magnetic navigation system
PMF	Precession magnetic field
RMF	Rotating magnetic field
SES	Self-expandable stent
USCy	Y-directional uniform saddle coil
USCz	Z-directional uniform saddle coil
UVCAP	Ultraviolet curable acrylic plastic

Manuscript received November 30, 2015; revised April 12, 2016 and May 15, 2016; accepted May 15, 2016. This work was supported by the National Research Foundation of Korea (NRF) grant funded by the Korean government (MSIP) (No. 2015R1A2A1A05001837).

W. Lee, J. Nam, B. Jang, and G. Jang (corresponding author) are with the Department of Mechanical Convergence Engineering, Hanyang University, Seoul 04763, Korea (e-mail: justinleews@gmail.com; njk0651@naver.com; stern89@naver.com; ghjang@hanyang.ac.kr).

I. INTRODUCTION

TUBULAR organs of a human body are gastrointestinal tracts, intestines, blood vessels, bronchial tubes, and urinary systems which are passage of substances. However, when they become narrowed due to cancer or fatty-substance deposit in the blood vessels, it can cause intestinal obstruction or myocardial infraction. Self-expandable stent (SES) is a popular medical device to widen narrowed regions and maintain expanded walls [1], [2]. The SES is made of shape-memory alloys compressed and covered by a catheter, so that they can self-expand when the catheter is uncovered. Conventional stent delivery methods using wired catheters have low steering ability and controllability, so that the success of stent deployment was mostly depended on the experience of medical doctors. Also, the medical doctors are constantly and directly exposed to radiation from X-ray scanners during the operation which increases risks of cancer, cataracts, and orthopedic strain [3]. Some commercial remote magnetic navigation systems such as *Niobe* (Sterotaxis, USA) and *CGCI* (Magnetecs, USA) have been developed to increase steering ability and controllability of the catheter and to reduce the radiation hazards of the medical doctor. However, they still have limitations of wired devices. For example, bacteria can permeate inside the body through catheter, and the risk increases higher when operation time becomes longer. This is called as Bacteremia, and the Bacteremia is one of the most common side effects of catheterization. It can be fatal to patients who have lower levels of immunity [4]. To overcome the limitations of wired devices, various medical robots and their wireless manipulation methods in tubular environments have been widely investigated.

Locomotion methods of the robots can be categorized into passive and active methods. The passive locomotion methods rely on the motion of external environments such as peristalsis of gastrointestinal tracts, and the active locomotion methods generate a propulsive force by controlling the motion of the robot [5]–[9]. Since high maneuverability and controllability are required to navigate in complicated and twisted tubular regions, the active locomotion methods are reasonable for navigation methods of the robots. Swimming with bioinspired moving fins [10]–[12] or helical structures [13]–[15] are

This article has been accepted for publication in a future issue of this journal, but has not been fully edited. Content may change prior to final publication. Citation information: DOI 10.1109/TIE.2016.2580126, IEEE Transactions on Industrial Electronics

common active locomotion methods. The swimming robots generate oscillating or rotating motions, which are converted to propulsive forces via the robot structures. However, these robots cannot stably maintain their current position under changes of the external environment because they do not make physical contact with the external walls. Locomotion utilizing friction forces between a robot and the external environment are the other effective active locomotion methods [16]–[19]. Robots utilizing these methods continuously make contact with the external walls during locomotion, resulting in the advantages of precise and stable manipulations. The crawling mechanism, which utilizes asymmetric friction forces, has the strong advantages of possessing a simple driving principle and maintaining position and orientation of the robot against motions of the environment such as heartbeat or peristalsis [20], [21]. Wireless powering methods of the robots can be categorized into electric and magnetic methods. The electric powering methods utilize electricity generated by built-in batteries or electromagnetic induction systems, and the magnetic powering methods utilize the magnetic torque and force generated by the interaction between built-in magnetic material of the robot and an external magnetic field (EMF). Since the magnetic powering methods can be fabricated as simple and small structures, miniaturized magnetic robots actuated by an EMF have been widely investigated for miniaturized medical robots [22], [23]. Based on these advantages of the crawling mechanisms and magnetic robots, several researchers have proposed crawling magnetic robots (CMR) and validated their effectiveness on navigating tubular environments [24], [25]. However, the conventional CMRs did not succeed in demonstrating diverse functions.

In this paper, we propose a novel CMR manipulated by a magnetic navigation system (MNS) for the navigation and wireless SES deployment in a narrowed tubular environment. The CMR is composed of a magnetic pulley module and a crawling module, as shown in Fig. 1. The MNS has three orthogonal pairs of electromagnetic coils, so that it can generate a three-dimensional uniform EMF by controlling the applied current. By utilizing the uniform EMF, the CMR can generate a crawling motion to navigate in tubular environments, simultaneous crawling and drilling motions to unclog blocked regions, and an uncovering motion of a stent cover to deploy the SES. We first describe the structures of the CMR and MNS. Then, we represent the selective motion control method and design processes with fabrication of the magnetic pulley module and crawling module. Finally, we assembled the prototyped CMR and conducted several experiments to show the validity of the proposed CMR and its manipulation methods.

II. Structures of the Crawling Magnetic Robot

Fig. 1 shows the proposed CMR composed of a magnetic pulley module and a crawling module. The magnetic pulley module that generates the pulling force consists of a pulley magnet with pulley arms, a module body, a moving pulley, wire, a SES with a stent cover, and a drill tip with an assembled magnet, as shown in Fig. 2(a). The pulley magnet is inserted in a magnet slot of the module body, with a gap in between. Then, the pulley arms are bonded to each side of the pulley magnet,

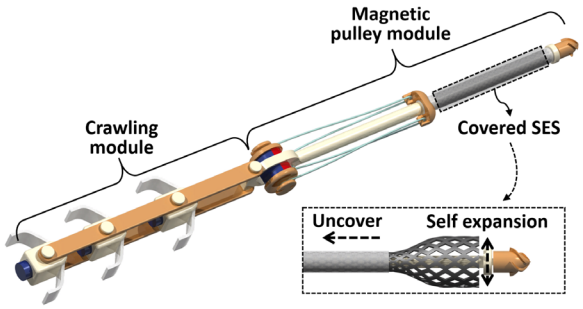

Fig. 1. Proposed CMR composed of a crawling module and a magnetic pulley module. A covered SES can be deployed by its self-expansion when it is uncovered.

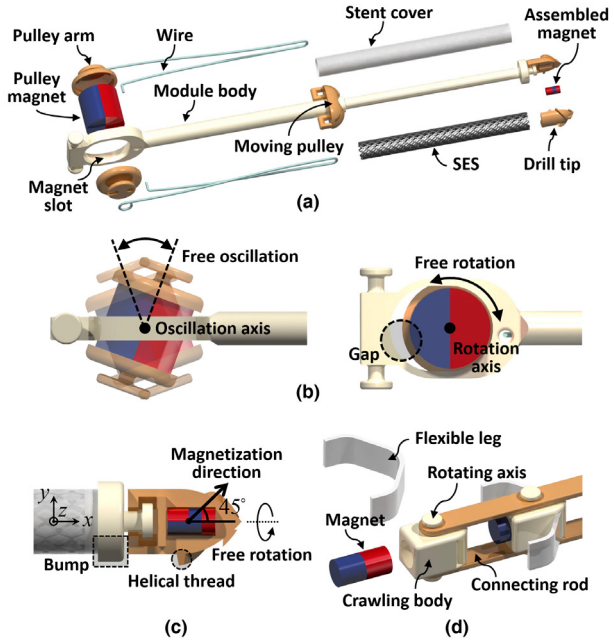

Fig. 2. (a) Structure of the magnetic pulley module. (b) Free oscillation and rotation of the pulley magnet with respect to each axis. (c) Cross-sectional view of the drill tip. (d) Structure of the crawling module.

and the moving pulley bonded with the stent cover is connected with the pulley arms through the wire. Since the bonded pulley arms structurally restrain the pulley magnet not to escape from the magnet slot, the pulley magnet can freely oscillate and rotate with respect to the rotating axis and oscillating axis, respectively, as shown in Fig. 2(b). This gap enables the pulley magnet not to deliver the magnetic torque to the module body during the crawling motions and to deliver the magnetic torque to the stent cover during the uncovering motions. The assembled magnet inserted in the drill tip is composed of two magnets which are axially and diametrically magnetized, as shown in Fig. 2(c). Since the assembled magnet has a total magnetization angle of 45°, the drill tip can rotate under a precession of the EMF. Also, the magnetic pulley module has a bump with a larger diameter than the stent cover at the front to protect the stent cover from impacts made during navigation. The crawling module consists of flexible legs, permanent magnets, crawling bodies, and two connecting rods, as shown in Fig. 2(d). Each crawling body has a permanent magnet and flexible leg, and the crawling bodies are linked by upper and lower connecting rods. The crawling body can rotate with

This article has been accepted for publication in a future issue of this journal, but has not been fully edited. Content may change prior to final publication. Citation information: DOI 10.1109/TIE.2016.2580126, IEEE Transactions on Industrial Electronics

TABLE I
MAJOR SPECIFICATIONS OF THE MNS

Coil type	Radius (mm)	Wire diameter (mm)	Coil turns
HC	216.0	1.0	430
USCy	167.5	1.2	400
USCz	133.8	1.2	320

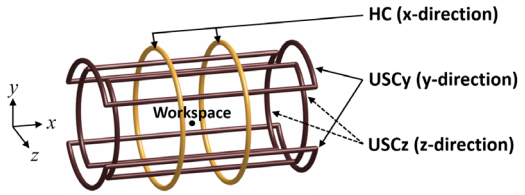

Fig. 3. Three orthogonal pairs of electromagnetic coils of the MNS.

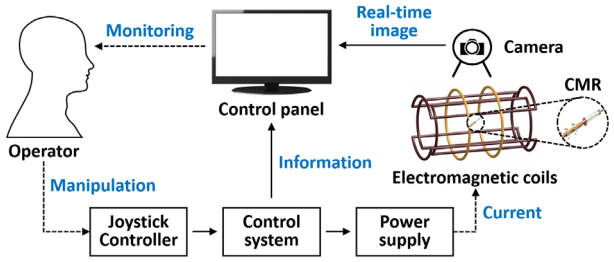

Fig. 4. System overview of the MNS.

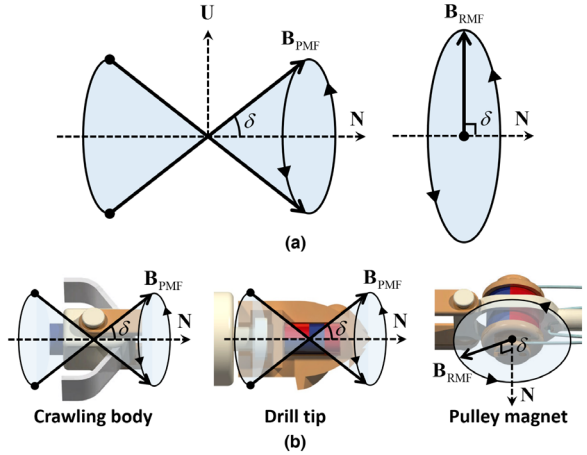

Fig. 5. (a) Trajectories of the PMF and RMF. (b) PMF to generate the crawling motion and simultaneous crawling and drilling motions and RMF to generate the uncovering motion.

respect to the rotating axis, so that it can rotate when external magnetic torque is applied.

III. SELECTIVE MOTION CONTROL METHOD

A. Magnetic Navigation System

The MNS has three orthogonal pairs of electromagnetic coils: an x-directional Helmholtz coil (HC), a y-directional uniform saddle coil (USCy), and a z-directional uniform saddle coil (USCz), as shown in Fig. 3. Since these pairs of coils are orthogonally arranged each other, the MNS can generate uniform EMF to any directions in three dimensional space by superposition of the uniform EMFs generated by each pair of coils. The pairs of coils with the specifications of Table I has cylindrical workspace with radius of 133 mm and length of 173 mm, and every point in the workspace have same magnitude and direction of the uniform EMF [26]. Therefore, if the CMR is manipulated within the workspace, the MNS can control motions of the CMR in three dimensions by controlling the applied uniform EMF which generates magnetic torque regardless of the position and orientation of the CMR. Fig. 4 shows a system overview of the MNS. An operator can monitor the motion of the CMR by acquired real-time image and the information of the MNS such as the applied current and the magnitude, frequency, and direction of the magnetic field. When the operator manipulates a joystick to control the motion of the CMR, the control system receives the signal, converts it into the current information for each electromagnetic coil and then transmits the information to the power supplies. Afterward, the power supplies apply the current to each electromagnetic coil to generate the uniform EMF. In this process, the MNS enables the operator to wirelessly control the CMR in real-time by open-loop control.

B. Principles of Manipulation

The uniform EMF generated by the MNS to control the motion of the CMR can be expressed as follows [26]:

$$\mathbf{B}_e = \left[0.7155\frac{i_h n_h}{r_h} \quad 0.6004\frac{i_{uy} n_{uy}}{r_{uy}} \quad 0.6004\frac{i_{uz} n_{uz}}{r_{uz}} \right]^T \tag{1}$$

where i_k, n_k, and r_k are the applied current, number of turns, and radius of the k^{th} coil, respectively. The number of turns and radius of each coil are presented in Table I, and the subscripts h, uy, and uz represent the HC, USCy, and USCz, respectively. A magnetic torque exerted on a permanent magnet under the uniform EMF can be expressed as follows:

$$\mathbf{T} = \mathbf{m} \times \mathbf{B}_e \tag{2}$$

where $\mathbf{m}$ is the magnetic moment of the permanent magnet. This magnetic torque can generate rotational motions of the magnet along the applied magnetic field. The uniform EMF to generate rotational motions of the CMR can be expressed as the following equation [13]:

$$\mathbf{B}_e = B_e(\cos\delta\mathbf{N} + \sin\delta\cos 2\pi ft\mathbf{U} + \sin\delta\sin 2\pi ft\mathbf{N}\times\mathbf{U}) \tag{3}$$

where B_e, δ, f, $\mathbf{N}$, and $\mathbf{U}$ are the magnitude, precession angle, rotational frequency of the uniform EMF, a unit vector of the rotating axis, and a unit vector normal to the $\mathbf{N}$, respectively. The uniform EMF can be classified as precession magnetic field (PMF, $0°<\delta<90°$) and rotating magnetic field (RMF, $\delta=90°$) according to δ, as shown in Fig. 5. By utilizing the PMF and RMF, the CMR can selectively generate the crawling motion, simultaneous crawling and drilling motions, and uncovering motion.

C. Crawling Motion

To navigate into the target narrowed region, the PMF is utilized to generate the crawling motion of the CMR, because the oscillating crawling bodies generate a propulsive force via an asymmetric friction force, as shown in Fig. 6 [24]. However, the applied PMF exerts magnetic torque not only on the magnets inserted in the crawling bodies, but also on the assembled magnet inserted in the drill tip and the pulley magnet

inserted in the module body. The magnetic torque exerted on the pulley magnet does not affect the motion of the module body due to the gap between the pulley magnet and the magnet slot, but the magnetic torque exerted on the assembled magnet of the drill tip can cause damage on the tubular environment by drilling motion of the drill tip. Since the magnetic moment of the magnet inserted in the crawling body is relatively larger than that of the assembled magnet, certain PMFs can generate large magnetic torque on the crawling bodies which can overcome their friction torque and small magnetic torque on the drill tip which cannot overcome its friction torque. Magnitude, precession angle, and rotational frequency of the PMF affect the motion of the CMR. The magnitude and precession angle of the PMF are related with the magnetic torque and the rotational frequency of the PMF is related with friction torque. According to a reference, the crawling motion is dominantly generated when the magnitude and precession angle of the PMF decreases and the rotational frequency of the PMF increases [25]. Thus, for safe navigation, the magnitude and precession angle of the PMF should be small, and the rotational frequency of the PMF should be high in order to generate the crawling motion without the drilling motion.

D. Simultaneous Crawling and Drilling Motions

When the CMR reaches a blocked region, the drilling motion of the drill tip is required to unclog the blockage. By generating relatively strong magnetic torque to overcome the friction torque exerted on both crawling bodies and drill tip, the CMR can generate simultaneous crawling and drilling motions. Since they generate a propulsive force which pushes the drill tip forward, they can unclog the blockage more effectively than only the drilling motion. The simultaneous crawling and drilling motions are dominantly generated when the magnitude and precession angle of the PMF increases and the rotational frequency of the PMF decreases [25].

E. Uncovering Motion

At the target narrowed region, the RMF is utilized to generate the uncovering motion of the stent cover to deploy the SES. The applied RMF exerts a magnetic torque not only on the pulley magnet, but also on the magnets inserted in the crawling bodies and the assembled magnets of the drill tip. However, the magnitude of the RMF should be maximized for the maximum pulling force; this controls the frequency of the RMF (not the magnitude of the RMF) in order to generate only the uncovering motion by utilizing the step-out frequency of the crawling bodies and drill tip. The step-out frequency is the maximum frequency that a magnet can move in sync with the frequency of the external magnetic field. Since the magnets of the crawling bodies and drill tip cannot be synchronized with an RMF with higher frequency than their step-out frequencies [27], the frequency of the RMF should be higher than their step-out frequencies to prevent the rotational motion of the crawling bodies and the drill tip. In the proposed CMR, the step-out frequency of the pulley magnet is higher than those of the magnets inserted in the crawling bodies and the assembled magnet inserted in the drill tip, mainly because the former is larger than the latter.

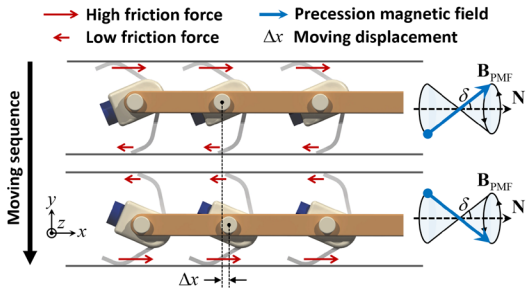

Fig. 6. Moving sequence of the crawling motion when the precession magnetic field sweeps in a counterclockwise direction.

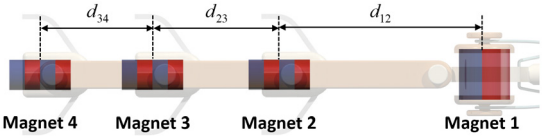

Fig. 7. Number of each inserted magnet and distances between the magnets. Magnet 1 is the pulley magnet, and Magnet 2 to 4 are the magnets inserted in the crawling bodies.

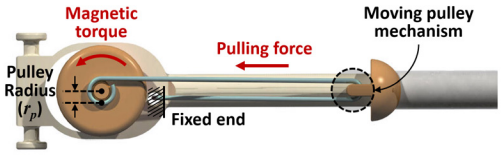

Fig. 8. Pulling force generated by the exerted magnetic torque and the moving pulley mechanism adopted to the magnetic pulley module.

IV. Design, Fabrication, and Assembly

A. Design of the Magnetic Pulley Module

Four magnets inserted in the CMR are affected not only by the uniform EMF, but also the internal magnetic field generated by each magnet, as shown in Fig. 7. In this case, the net torque for the n^{th} magnet can be expressed as the following equation:

$$T_{n,\text{net}} = T_{n,e} - \sum_{m=1}^{4} T_{n,m} - T_f \quad (\text{for } n = 1 \text{ to } 4,\ n \neq m) \tag{4}$$

where $T_{n,e}$, $T_{n,m}$, and T_f are the external magnetic torque generated by the PMF, the internal magnetic torque generated by the m^{th} magnet, and the friction torque exerted on the n^{th} magnet, respectively. For the uncovering motion of the stent cover, the pulling force generated by the pulley magnet (n=1) should be larger than the friction force between the SES and stent cover. The net torque of the pulley magnet converted to the pulling force can be expressed as follows:

$$T_{1,\text{net}} = T_{1,e} - \sum_{m=2}^{4} T_{1,m} - T_{f,p} = F_{\text{pull}} r_p \tag{5}$$

where $T_{f,p}$, F_{pull}, and r_p are the friction torque generated at the pulley magnet, converted pulling force, and pulley radius, respectively. To amplify F_{pull} without increasing the size of the pulley magnet, a moving pulley mechanism is adopted, as shown in Fig. 8. Since the pulley magnet has its maximum net torque when the external torque is maximized and the internal torque becomes zero, the maximum amplified pulling force converted from the net torque can be expressed as the following equations, using (2), (3), and (5):

This article has been accepted for publication in a future issue of this journal, but has not been fully edited. Content may change prior to final publication. Citation information: DOI 10.1109/TIE.2016.2580126, IEEE Transactions on Industrial Electronics

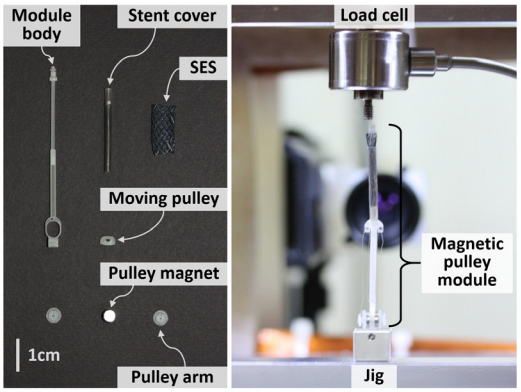

Fig. 9. Fabricated parts to specify the constraint of the pulley magnet. (a) Parts of the magnetic pulley module. (b) Load cell and jig to measure the friction and pulling forces.

$$F^*_{\text{pull,max}} = \alpha F_{\text{pull,max}} = \frac{\alpha(m_p B_e - T_{f,p})}{r_p} \tag{6}$$

where α, $F_{\text{pull, max}}$, and m_p are the amplification factor caused by the moving pulley mechanism, the maximum unamplified pulling force, and the magnitude of the magnetic moment of the pulley magnet, respectively. $F^*_{\text{pull, max}}$ should be larger than the maximum friction force ($F_{s,\text{max}}$) for the uncovering motion of the stent cover. Therefore, a constraint of the pulley magnet can be derived from (6) as follows.

$$m_p > \frac{r_p F_{s,\max} + \alpha T_{f,p}}{\alpha B_e} \tag{7}$$

To determine the minimum magnetic moment of the pulley magnet for the compact design of the CMR, $F_{s,\text{max}}$, α, and $T_{f,p}$ were obtained via experimental measurements. We fabricated parts of the magnetic pulley module by using 3D printing technology with an ultraviolet curable acrylic plastic (UVCAP) material, as shown in Fig. 9. As a result, r_p was determined to be 0.6 mm due to the fabricating limitation of the UVCAP. A Niti-S Vascular Stent and catheter (TaeWoong Medical, Korea) were used for the SES and stent cover, and the SES had a diameter of 10 mm and a length of 15 mm when fully expanded. The maximum RMF (B_e=14 mT) was applied to generate the magnetic torque on the pulley magnet via the constructed MNS, and a load cell (Honeywell, USA) with an oscilloscope was utilized to measure and record the forces, as shown in Fig. 10. Fig. 11(a) presents the experimental setup used to measure the friction force between the stent cover and the SES. When the magnetic torque is applied, it is converted to a pulling force in order to pull the stent cover downward. This uncovering motion causes a friction force between the stent cover and the SES, so that the load cell can measure the friction force. Fig. 11(b) represents the experimental setup to measure the unamplified and amplified pulling force. Since a connector joins the stent cover and load cell axis, the load cell can measure the pulling force generated by the magnetic torque. As a result, $F_{s,\text{max}}$, $F_{\text{pull, max}}$, and $F^*_{\text{pull, max}}$ were measured as 1.12 N, 0.99 N, and 1.85 N, respectively, as shown in Fig. 12. Further, α and $T_{f,p}$ were obtained by (6) as 1.86 and 0.96 mN·m, respectively. Therefore, the minimum magnetic moment of the pulley magnet was calculated to be 0.0898 A·m^2 by (7), where

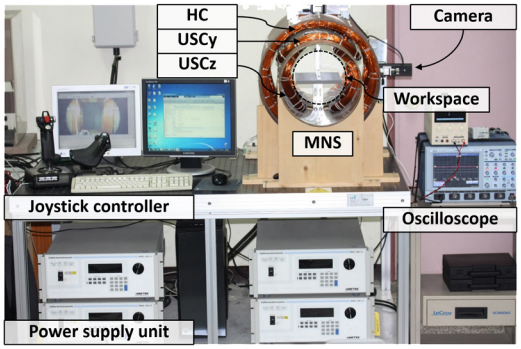

Fig. 10. Experimental setup and constructed MNS.

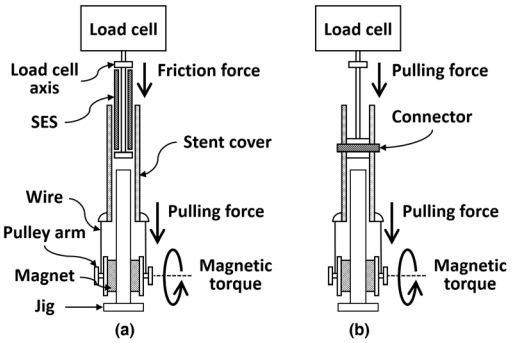

Fig. 11. (a) Experimental setup to measure the maximum friction force. (b) Experimental setup to measure the unamplified and amplified pulling forces.

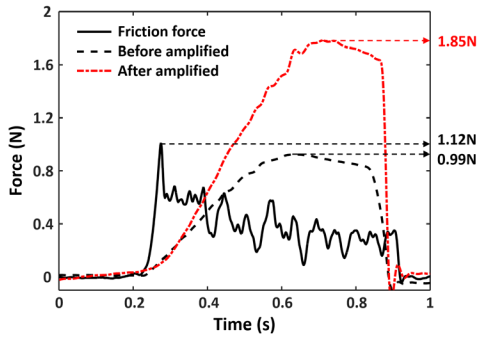

Fig. 12. Comparison between the measured friction force, unamplified pulling force, and amplified pulling force.

we used the pulley magnet presented in Table II which satisfies this constraint.

B. Design of the Crawling Module

For the compact structure of the crawling module, the sum of the distances between magnets presented in Fig. 7 should be minimized. However, two constraints should be considered. First, the external magnetic torque exerted on each crawling body should be high enough to overcome the internal magnetic torque and friction torque for the crawling motion to generate an asymmetric friction force. Utilizing a point-dipole model, a magnetic field generated by a permanent magnet can be expressed as follows [28]:

$$\mathbf{B}_{\text{point-dipole}} = \frac{\mu_0}{4\pi}\left(\frac{3\mathbf{R}(\mathbf{m}\cdot\mathbf{R})}{R^5} - \frac{\mathbf{m}}{R^3}\right) \tag{8}$$

where μ_0, $\mathbf{R}$, and R are the permeability of free space, the vector from the magnet to a point, and the magnitude of this vector,

This article has been accepted for publication in a future issue of this journal, but has not been fully edited. Content may change prior to final publication. Citation information: DOI 10.1109/TIE.2016.2580126, IEEE Transactions on Industrial Electronics

TABLE II
DESIGN VARIABLES OF THE CMR

Name	Variable	Value (mm)
Distances between magnets	d_{12}	15.0
	d_{23}	13.8
	d_{34}	11.5
Assembled magnet	Diameter	1.0
	Length	1.8
Pulley magnet	Diameter	5.0
	Length	5.0
Magnets inserted in the crawling module	Diameter	3.0
	Length	6.0

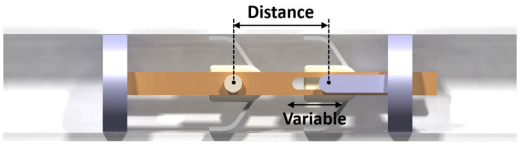

Fig. 13. Setup to measure the distance between the crawling bodies.

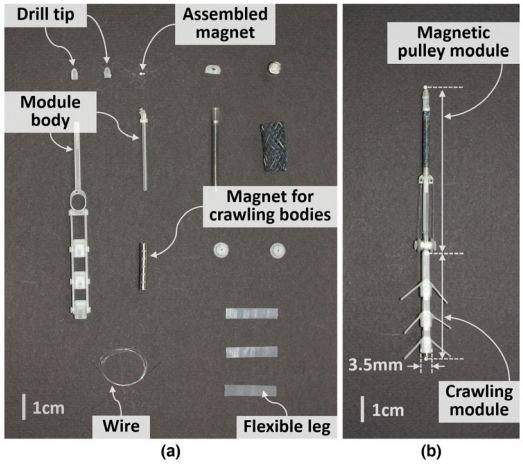

Fig. 14. (a) Prototyped parts, magnets, flexible legs, and wire. (b) Assembled CMR.

respectively. Second, each distance between the crawling bodies should be larger than the minimum distance ($d_{\min}$) to change the moving direction backward. When the CMR changes the moving direction by rotating the crawling bodies with respect to each rotating axis, the flexible legs are easily tangled together if $d_{\min}$ is too short. Therefore, the distances between the crawling bodies can be obtained by the following optimization problem:

$$\text{Minimize} \quad d_{12} + d_{23} + d_{34} \tag{9}$$

$$\text{Subject to} \quad T_{n,e} > \sum_{m=1}^{4} T_{n,m} - T_{f,c} \quad (\text{for } n = 2 \text{ to } 4,\ n \neq m) \tag{10}$$
$$d_{12}, d_{23}, \text{and } d_{34} \geq d_{\min}$$

where $T_{f,c}$ is the friction torque generated at the crawling body. Since $T_{n,e}$ and $T_{n,m}$ can be calculated by substituting (3) and (8) into (2), respectively, $T_{f,c}$ can be determined by measuring the distance between the two crawling bodies when the net torque becomes zero under the given uniform EMF, as shown in Fig. 13. Also, $d_{\min}$ can be determined by varying the distance between the two crawling bodies, in order to find the minimum distance which allows change of the moving direction without tangling the flexible legs. As a result, $T_{f,c}$ was calculated to be 0.135 mN·m, and $d_{\min}$ was determined to be 11.5 mm. Therefore, the distances between the crawling bodies were optimized by (9) and (10) using MATLAB's *fmincon* optimization function. The obtained distances are presented in Table II.

C. Assembled Crawling Magnetic Robot

Finally, we prototyped and assembled all modules of the CMR, as shown in Fig. 14. All magnets are NdFeB with a magnetization of 1,130,000 A/m, and Table II shows the design variables of the CMR. The flexible legs made of silicone rubber with a length of 20 mm were used, and the wire made of acrylic plastic with a diameter of 0.1 mm was used.

V. EXPERIMENT

First, we observed the crawling and drilling motions of the CMR under various PMF conditions. Fig. 15(a), (b), and (c) present the observed motions under the PMF frequencies of 5 Hz, 10 Hz, and 15 Hz, respectively. To generate only the crawling motion for safe navigation, the magnitude and precession angle of the PMF should be relatively small and the rotational frequency of the PMF should be relatively high, as shown in Fig. 15(b) and (c). On the other hand, to generate the simultaneous crawling and drilling motions to unclog the blockage, the magnitude and precession angle of the PMF should be relatively large and the rotational frequency of the PMF should be relatively low as shown in Fig. 15(a) and (b).

Second, we measured the step-out frequency of the crawling bodies and the drill tip under the RMF to specify conditions of the RMF for selective uncovering motion. The measured step-out frequencies of the crawling bodies and drill tip were 8 Hz and 5 Hz, respectively, and their motions became negligible when the frequency of the RMF increased to 12 Hz. Fig. 16(a) shows unintended rotational motions of the crawling bodies generated by the RMF with lower frequency than their step-out frequency, and Fig. 16(b) shows successful uncovering motion of the stent cover generated by the RMF with 15 Hz which is higher than step-out frequency of the crawling bodies.

Finally, an experiment was conducted in a Y-shaped glass tube filled with water to verify the CMR and its manipulation methods, as shown in Fig. 17. The glass tube has inner diameter of 10 mm and completely blocked by a pseudo blood clot made of 5% agar. The applied PMF and RMF conditions for selective motions of the CMR were selected based upon the experimental results in Fig. 15 and 16. The CMR was moved forward by the crawling motion under small magnitudes of the PMF (Step 1: θ=-30°, ϕ=90°, δ=45°, B_0=8 mT, f=10 Hz), and changed direction into a lower branch to navigate toward the target region (Step 2: θ=0°, ϕ=90°, δ=45°, B_0=8 mT, f=10 Hz). Here, θ and ϕ are the angle between the rotating axis (**N**) of the uniform EMF and the x-direction and y-direction, respectively. Then, the CMR simultaneously generated the crawling and drilling motions under the large magnitude of the PMF in order to unclog the pseudo blood clot (Step 3: θ=0°, ϕ=90°, δ=45°, B_0=14 mT, f=10 Hz). Finally, the CMR deployed the SES by

This article has been accepted for publication in a future issue of this journal, but has not been fully edited. Content may change prior to final publication. Citation information: DOI 10.1109/TIE.2016.2580126, IEEE Transactions on Industrial Electronics

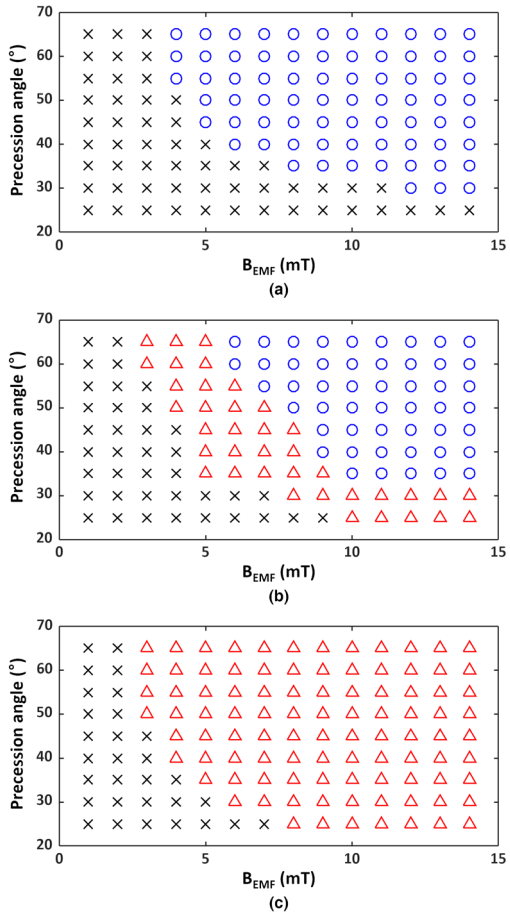

Fig. 15. Crawling motions and simultaneous crawling and drilling motions of the CMR according to changes of the precession angle, magnitude, and frequency of the PMF (×: No motion, ○: Simultaneous crawling and drilling motions, △: crawling motion). (a) Case of 5 Hz. (b) Case of 10 Hz. (c) Case of 15 Hz.

the uncovering motion under the high frequency of the RMF, as shown in Fig. 18(a) (Step 4: θ=90°, ϕ=90°, B_0=14 mT, f=15 Hz). Fig. 18(b) shows the narrowed region with a pseudo blood clot, and Fig. 18(c) shows the unclogged and widened region resulting from the drilling and deployment of the SES. After the SES deployment, the CMR inverted its moving direction by rotating the **N** of the uniform EMF along the y-axis (Step 5). When the external magnetic field is rotated 180 degrees, the leg position changes because the magnets of the crawling bodies tend to align along the magnetic field direction. Then, the CMR moved back to the branch (Step 6: θ=180°, ϕ=90°, δ=45°, B_0=8 mT, f=10 Hz) and the starting point (Step 7: θ=150°, ϕ=90°, δ=45°, B_0=8 mT, f=10 Hz) via the crawling motion. Therefore, the proposed novel CMR system can deliver the SES by controlling the selective motions in narrowed tubular environments such as Arteria femoralis, Iliac artery, and Subclavian artery which have anatomically similar inner diameter of the glass tube in this experiment.

VI. Conclusion

We proposed a novel CMR manipulated by the MNS for the wireless SES delivery in narrowed tubular environments. By utilizing the uniform EMF, the proposed CMR can generate the

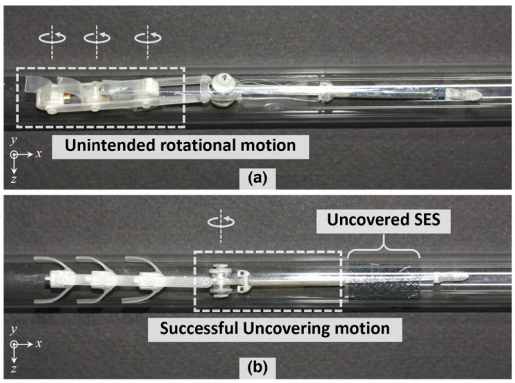

Fig. 16. (a) Rotational motions of the crawling bodies under RMF with lower frequency (6 Hz) than the step-out frequency. (b) Stable uncovering motion of the CMR under RMF with higher frequency (15 Hz) than the step-out frequency.

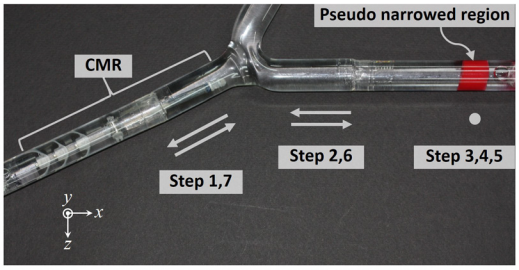

Fig. 17. Experimental sequence of the crawling and uncovering motion of the proposed CMR.

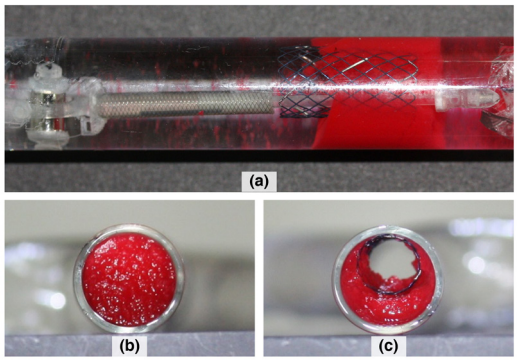

Fig. 18. (a) The CMR deploys the SES by the uncovering motion of the stent cover to widen the narrowed region. (b) Before the SES deployment. (c) After the SES deployment.

crawling motion to navigate in tubular environments, the simultaneous crawling and drilling motions to unclog the blocked region, and the uncovering motion of a stent cover to deploy the SES. We described structures of the CMR and MNS, the selective motion control method, and the design processes with fabrication. Also, the CMR and its manipulation methods were verified by the several experiments. There are still several design, control, and safety issues of the proposed CMR system such as miniaturization of the CMR, independent control of the drilling motion, improvements of the MNS to increase the size and power, and clinical validation before they will be applied to a human body. However, this research can contribute to extending applications of the magnetic robots for wireless stent delivery to replace the conventional operations using wired catheters.

REFERENCES

[1] J. H. Rogers and J. R. Laird, "Overview of new technologies for lower extremity revascularization," *Circulation*, vol. 116, no. 18, pp. 2072–2085, Oct. 2007.

[2] P. H. P. Davids, A. K. Groen, E. A. J. Rauws, G. N. J. Tytgat, and K. Huibregtse, "Randomised trial of self-expanding metal stents versus polyethylene stents for distal malignant biliary obstruction," *The Lancet*, vol. 340, no. 8834–8835, pp. 1488–1492, Dec. 1992.

[3] E. Picano, E. Vano, L. Domenici, M. Bottai, and I. Thierry-Chef, "Cancer and non-cancer brain and eye effects of chronic low-dose ionizing radiation exposure," *BMC Cancer*, vol. 12, p. 157, 2012.

[4] M. H. Samore, M. A. Wessolossky, S. M. Lewis, S. J. Shubrooks Jr, and A. W. Karchmer, "Frequency, Risk Factors, and Outcome for Bacteremia After Percutaneous Transluminal Coronary Angioplasty," *Am. J. Cardiol.*, vol. 79, no. 7, pp. 873–877, Apr. 1997.

[5] L. Yan, T. Wang, D. Liu, J. Peng, Z. Jiao, and C.-Y. Chen, "Capsule robot for obesity treatment with wireless powering and communication," *IEEE Trans. Ind. Electron.*, vol. 62, no. 2, pp. 1125–1133, Feb. 2015.

[6] R. Carta, G. Tortora, J. Thoné, B. Lenaerts, P. Valdastri, A. Menciassi, P. Dario, and R. Puers, "Wireless powering for a self-propelled and steerable endoscopic capsule for stomach inspection," *Biosens. Bioelectron.*, vol. 25, no. 4, pp. 845–851, Dec. 2009.

[7] M. Simi, P. Valdastri, C. Quaglia, A. Menciassi, and P. Dario, "Design, fabrication, and testing of a capsule with hybrid locomotion for gastrointestinal tract exploration," *IEEE/ASME Trans. Mechatron.*, vol. 15, no. 2, pp. 170–180, Apr. 2010.

[8] S. H. Kim and K. Ishiyama, "Magnetic robot and manipulation for active-locomotion with targeted drug release," *IEEE/ASME Trans. Mechatron.*, vol. 19, no. 5, pp. 1651–1659, Oct. 2014.

[9] S. Yim and M. Sitti, "Design and rolling locomotion of a magnetically actuated soft capsule endoscope," *IEEE Trans. Robot.*, vol. 28, no. 1, pp. 183–194, Feb. 2012.

[10] L. Wen, T. Wang, G. Wu, J. Liang, and C. Wang, "Novel method for the modeling and control investigation of efficient swimming for robotic fish," *IEEE Trans. Ind. Electron.*, vol. 59, no. 8, pp. 3176–3188, Aug. 2012.

[11] X. Niu, J. Xu, Q. Ren, and Q. Wang, "Locomotion learning for an anguilliform robotic fish using central pattern generator approach," *IEEE Trans. Ind. Electron.*, vol. 61, no. 9, pp. 4780–4787, Sep. 2014.

[12] S. Guo, T. Fukuda, and K. Asaka, "A new type of fish-like underwater microrobot," *IEEE/ASME Trans. Mechatron.*, vol. 8, no. 1, pp. 136–141, Mar. 2003.

[13] S. M. Jeon, G. H. Jang, H. C. Choi, S. H. Park, and J. O. Park, "Magnetic navigation system for the precise helical and translational motions of a microrobot in human blood vessels," *J. Appl. Phys.*, vol. 111, no. 7, p. 07E702, Apr. 2012.

[14] S. M. Jeon, G. H. Jang, and W. S. Lee, "Drug-enhanced unclogging motions of a double helical magnetic micromachine for occlusive vascular diseases," *IEEE Trans. Magn.*, vol. 50, no. 11, pp. 1–4, Nov. 2014.

[15] W. Lee, S. Jeon, J. Nam, and G. Jang, "Dual-body magnetic helical robot for drilling and cargo delivery in human blood vessels," *J. Appl. Phys.*, vol. 117, no. 17, p. 17B314, May 2015.

[16] J. Park, D. Hyun, W.-H. Cho, T.-H. Kim, and H.-S. Yang, "Normal-force control for an in-pipe robot according to the inclination of pipelines," *IEEE Trans. Ind. Electron.*, vol. 58, no. 12, pp. 5304–5310, Dec. 2011.

[17] H.-P. Huang, J.-L. Yan, and T.-H. Cheng, "Development and fuzzy control of a pipe inspection robot," *IEEE Trans. Ind. Electron.*, vol. 57, no. 3, pp. 1088–1095, Mar. 2010.

[18] Y.-S. Kwon and B.-J. Yi, "Design and motion planning of a two-module collaborative indoor pipeline inspection robot," *IEEE Trans. Robot.*, vol. 28, no. 3, pp. 681–696, Jun. 2012.

[19] K. Nagaya, T. Yoshino, M. Katayama, I. Murakami, and Y. Ando, "Wireless piping inspection vehicle using magnetic adsorption force," *IEEE/ASME Trans. Mechatron.*, vol. 17, no. 3, pp. 472–479, Jun. 2012.

[20] J. A. Galvez, P. Gonzalez de Santos, and F. Pfeiffer, "Intrinsic tactile sensing for the optimization of force distribution in a pipe crawling robot," *IEEE/ASME Trans. Mechatron.*, vol. 6, no. 1, pp. 26–35, Mar. 2001.

[21] Z. Wang and H. Gu, "A bristle-based pipeline robot for ill-constraint pipes," *IEEE/ASME Trans. Mechatron.*, vol. 13, no. 3, pp. 383–392, Jun. 2008.

[22] B. J. Nelson, I. K. Kaliakatsos, and J. J. Abbott, "Microrobots for minimally invasive medicine," *Annu. Rev. Biomed. Eng.*, vol. 12, no. 1, pp. 55–85, Apr. 2010.

[23] M. Sitti, H. Ceylan, W. Hu, J. Giltinan, M. Turan, S. Yim, and E. Diller, "Biomedical applications of untethered mobile milli/microrobots," *Proc. IEEE*, vol. 103, no. 2, pp. 205–224, Feb. 2015.

[24] J. Nam, S. Jeon, S. Kim, and G. Jang, "Crawling microrobot actuated by a magnetic navigation system in tubular environments," *Sens. Actuators Phys.*, vol. 209, pp. 100–106, Mar. 2014.

[25] S. J. Kim, G. H. Jang, S. M. Jeon, and J. K. Nam, "A crawling and drilling microrobot driven by an external oscillating or precessional magnetic field in tubular environments," *J. Appl. Phys.*, vol. 117, no. 17, p. 17A703, May 2015.

[26] S. Jeon, G. Jang, H. Choi, and S. Park, "Magnetic navigation system with gradient and uniform saddle coils for the wireless manipulation of micro-robots in human blood vessels," *IEEE Trans. Magn.*, vol. 46, no. 6, pp. 1943–1946, Jun. 2010.

[27] A. W. Mahoney, N. D. Nelson, K. E. Peyer, B. J. Nelson, and J. J. Abbott, "Behavior of rotating magnetic microrobots above the step-out frequency with application to control of multi-microrobot systems," *Appl. Phys. Lett.*, vol. 104, no. 14, p. 144101, Apr. 2014.

[28] A. J. Petruska and J. J. Abbott, "Optimal permanent-magnet geometries for dipole field approximation," *IEEE Trans. Magn.*, vol. 49, no. 2, pp. 811–819, Feb. 2013.

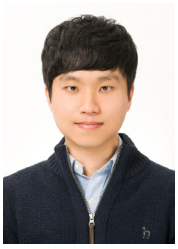

Wonseo Lee (S'16) received the B.S. in Mechanical Engineering from Hanyang University, Seoul, Korea in 2014. He is currently working toward the Ph.D. degree in Mechanical Convergence Engineering at Hanyang University, Seoul, Korea.

His current research interest includes design, analysis, and control of magnetic robots and magnetic catheters with electromagnetic systems for biomedical applications.

Jaekwang Nam is a graduate student in the department of Mechanical Convergence Engineering at Hanyang University, Seoul, Korea. He received his B.S. in Mechanical Engineering from Hanyang University in 2011.

His research interests are various structures of the microrobots performing multifunction in human blood vessels by magnetic navigation system.

Bongjun Jang received his B.S. in Mechanical Engineering from Gachon University, Gyeonggi-do, Korea in 2015. He is currently working toward the M.S. degree in Mechanical Convergence Engineering at Hanyang University, Seoul, Korea.

His current research interest includes design, analysis, and control of magnetic robots and electromagnetic systems for biomedical applications.

Gunhee Jang (M'00) received the B.S. in Mechanical Engineering from Hanyang University, Seoul, Korea in 1984, the M.S. in Mechanical Engineering from Korea Advanced Institute of Science and Technology (KAIST), Seoul, Korea in 1986 and the Ph.D. in Mechanical Engineering from University of California, Berkeley, USA in 1993. He is a professor in the Department of Mechanical Engineering and the director of the Precision Rotating Electromechanical Machine Laboratory (PREM) in Hanyang University, Seoul, Korea.

His current research is focused on the microrobot actuated by magnetic navigation system, electromechanical systems such as motors and actuators. He has authored or coauthored over 280 articles published in journals and conferences in his field and over 29 patents including several international patents.